Met. Mater. Int., Vol. 21, No. 4 (2015), pp. 659~665
doi: 10.1007/s12540-015-4627-z

Tensile and Creep Deformation of a Newly Developed Ni-Fe-Based Superalloy for 700 °C Advanced Ultra-Supercritical Boiler Applications

Y. Yuan[1,*], Z. H. Zhong[2,*], Z.S. Yu[3,1], H. F. Yin[1], Y. Y. Dang[1], X. B. Zhao[1], Z. Yang[1], J. T. Lu[1], J. B. Yan[1], and Y. Gu[1]

[1]Xi'an Thermal Power Research Institute Co. Ltd., No. 136, Xingqing Road, Xi'an 710032, China
[2]School of Materials Science and Engineering, Hefei University of Technology, No.193, Tunxi Road, Hefei 230009, China
[3]State Key Laboratory for Mechanical Behavior of Materials, Xi'an Jiaotong University, Xi'an 710049, China

(received date: 20 December 2014 / accepted date: 19 March 2015)

A new Ni-Fe-based superalloy, HT-X, has been developed for applications in 700 °C advanced ultra-supercritical (A-USC) boilers. The HT-X alloy is subjected to various heat treatments. Tensile tests are conducted at room temperature (RT), 700 °C and 750 °C. Creep tests are carried out under conditions of 700 °C/300 MPa and 750 °C/150 MPa. After aging treatment, the yield strength of the HT-X alloy at RT and 750 °C is 787 MPa and 624 MPa, respectively. When additional thermal exposure at 750 °C for 5400 h is applied, the yield strength is decreased to 656 MPa at RT and 480 MPa at 700 °C. For an aged specimen, the *a*/2<110> dislocation shearing process occurs when tensile testing is conducted at RT and 750 °C. As the γ' precipitate size increases in the specimen that is thermally exposed at 750 °C for 5400 h, Orowan bowing is the dominant dislocation process, and stacking faults develop in the γ' precipitates at both RT and 700 °C. Dislocation slip combined with climb is the dominant mechanism under the creep testing conditions. The factors that affect the mechanical properties and deformation mechanisms are discussed.

Keywords: Ni-Fe-based, alloys, forging, mechanical properties, transmission electron microscopy (TEM)

1. INTRODUCTION

In coal-fired power plants, increasing steam temperature and pressure is an effective method for improving thermal efficiency and for reducing coal consumption as well as CO_2 and NO_x emissions. The current 600 °C ultra-supercritical power plants typically have a steam pressure of 25-28 MPa, and the net thermal efficiency is approximately 43-45%. By contrast, 700 °C advanced ultra-supercritical (A-USC) power plants with a steam pressure of 30-35 MPa can achieve a net thermal efficiency of above 50% [1]. Currently these 700 °C A-USC technologies are being developed by the USA, Europe, Japan, China and India.

The effective implementation of 700 °C A-USC boiler and steam turbine technologies relies on the development and manufacturing of materials for high temperature components. The super-heater and reheater are the components in the 700 °C A-USC boilers that withstand the most severe service conditions. These components require a rupture life of 10^5 h while maintaining a rupture strength of greater than 100 MPa operating at 750 °C (the metal temperature is set to be 50 °C higher than steam temperature, according to the design standard of power plants in China). The temperature capability of the most advanced ferritic and austenitic heat resistant steels is around 650 °C and 700 °C, respectively [2,3]. Thus, they cannot meet the requirements of super-heater and reheater in 700 °C A-USC boilers. Ni-based superalloys, such as 740/740H [4-7], CCA617 [8-10], Haynes 282 [11] and Nimonic 263 [12], are promising candidates for 700 °C A-USC boiler applications. However, Ni-based alloys are much more expensive than heat-resistant steels. Therefore, Ni-Fe-based alloys (e.g., HR6W, HR35 and GH984G) have been developed in light of both their high temperature mechanical properties and lower cost. The precipitation strengthening in HR6W [13], HR35 [14] and GH984G [15] is mainly contributed by the Laves phase, α-Cr, and γ' phase, respectively.

Recently, a new Ni-Fe-based superalloy (designated as HT-X hereafter) has been developed at the Xi'an Thermal Power Research Institute Co. Ltd., China [16]. This new alloy has comparable creep strength to Inconel 740H, but better hot workability and lower cost due to more than 20 wt%

*Corresponding author: yuanyong@tpri.com.cn, zhong@hfut.edu.cn

addition of Fe [17]. The HT-X alloy is designed to be used in the temperature range of 700-750 °C. Before this promising new alloy can be implemented in A-USC applications, it is necessary to understand the deformation behavior under various conditions. Previous investigations (Ref. [16]) studied the compressive behavior of HT-X alloy after aging treatment, aging treatment plus 1000 h and 7000 h of thermal exposure at 700 °C, and compressive tests that were carried out at 700 °C. In the present study, the tensile and creep deformation microstructures of HT-X alloy after various heat treatments were investigated. Compared with the previous investigations, the present study showed different deformation microstructures. The results are beneficial for further understanding of the relationships between the mechanical properties and microstructures in the HT-X alloy and for improving the design of A-USC alloys.

2. EXPERIMENTAL PROCEDURES

A 7 kg Ni-Fe-based HT-X alloy ingot, of chemical composition Ni-(20-30)wt%Fe-(18-25)wt%Cr-(3-7)wt%Ti+Al, was prepared via vacuum induction melting. The ratio of Ti/Al was controlled to be in the range of 1.0-1.3. The ingot was homogenized, hot forged, and rolled at 1200 °C. Finally, a 10 mm thick plate was attained. All the test specimens used in this study were cut from this plate in the longitudinal direction. The alloy specimen used for testing was first solutioned at 1100 °C for 1 h. Then, an aging treatment (designated as H1A1) was carried out at 750 °C for 8 h, then furnace cooled at 50 °C/h to 650 °C, and held at 650 °C for 16 h with subsequent air cooling.

Tensile testing was conducted using specimens that had undergone an aging treatment or an aging treatment plus long-term thermal exposure at 750 °C for 5400 h. The cylindrical tensile specimen had a size of 3 mm in diameter and 16 mm in gauge length. Tensile tests were performed at an initial strain rate of 2.0×10^{-4} s^{-1} up to about 3% strain, and then strain rate was increased from 1.0 to 5.0×10^{-3} s^{-1} until the specimen fractured. Tests were conducted at room temperature (RT), 700 °C and 750 °C in air. For each condition, two samples were tested, and the average results were used for discussion.

For creep testing, the specimens first underwent aging treatment or aging treatment plus thermal exposure at 800 °C for 4 h. The cylindrical creep specimen had a size of 4 mm in diameter and 22 mm in gauge length. Creep tests were conducted at 700 °C/300 MPa and 750 °C/150 MPa. One sample was tested at each condition.

The initial microstructures after various heat treatments were examined using scanning electron microscopy (SEM). The microstructures after mechanical testing were characterized using transmission electron microscopy (TEM; Tecnai 20 operating at 200 kV). TEM discs cut perpendicular to the stress axis were manually ground to about 50 μm, and then perforated by a twin-jet electro-polisher at 40 V/18 mA and -10 °C. The electrolyte consisted of 225 ml acetic acid, 225 ml butylcellosolve and 50 ml perchloric acid.

3. RESULTS AND DISCUSSION

3.1. Mechanical properties

The tensile properties of the HT-X alloy are shown in Table 1. For comparison, the yield strength ($\sigma_{0.2}$) of aging treated Nimonic 263 [18] is also listed in Table 1. After aging treatment, the yield strength of HT-X at RT and 750 °C was 787 MPa and 624 MPa, respectively. The elongation (δ) and area reduction (ψ) decreased with increasing temperature. This could be related to grain boundary (GB) strength because with increasing temperature, dislocation motion in the grain interior becomes easier due to thermal activation. Thus, many dislocations accumulate at the GBs and cause stress concentration. The GB strength decreases with increasing temperature. Insufficient GB strength may accelerate tensile failure at a relatively lower elongation and area reduction.

For the specimens after long term thermal exposure at 750 °C for 5400 h, the yield strength of HT-X decreased to 656 MPa at RT and 480 MPa at 700 °C. The elongation and area reduction increased with increasing temperature. The variation of ultimate tensile strength (UTS) has the same trend as yield strength. Note that the HT-X alloy showed comparable yield strength with Nimonic 263 even after long-term thermal exposure at 750 °C for 5400 h.

The entire creep curves of HT-X under various creep conditions are illustrated in Fig. 1(a). At 700 °C and 300 MPa, the H1A1 treated specimen had a longer creep life than that with H1A1 treatment plus 4 h of thermal exposure at 800 °C. However, up to roughly 220 h, the thermally exposed specimen had a lower creep strain than the H1A1 treated specimen, as seen in Fig. 1(b). At 750 °C and 150 MPa, the H1A1

Table 1. Tensile properties of the HT-X alloy

Heat treatment	Temperature (°C)	$\sigma_{0.2}$ (MPa)	UTS (MPa)	δ (%)	ψ (%)
H1A1[a]	RT	787	1192	24	29
H1A1 + 750 °C/5400 h	RT	656	1095	16	18
H1A1	750	624	725	12	12
H1A1 + 750 °C/5400 h	700	480	638	22	32
Nimonic 263, Aged [18]	700	490	-	-	-

[a]H1A1 denotes the aging heat treatment.

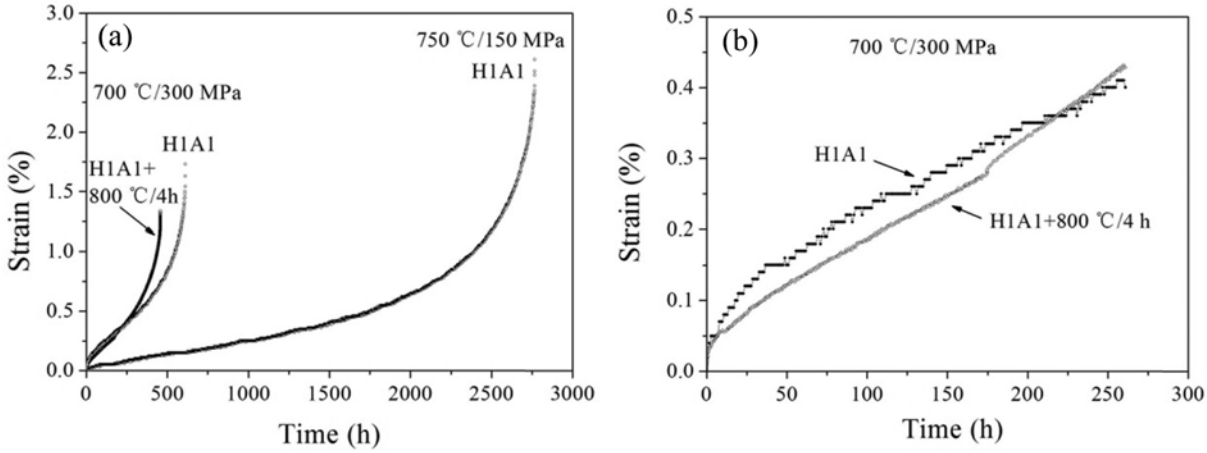

Fig. 1. Creep curves of HT-X at 700 °C/300 MPa and 750 °C/150 MPa after various heat treatments displayed for (a) the entire creep time until failure and (b) the initial creep stage to 250 h.

treated specimen had a creep life of 2768 h. For all three specimens, the total creep strain was less than 3.0%.

3.2. Initial microstructures after various heat treatments

The initial microstructures of the HT-X alloy specimens after various heat treatments are illustrated in Fig. 2. The grain size of HT-X after aging treatment was about 135 μm (see Fig. 2(a)). The alloy mainly consisted of $M_{23}C_6$ type carbides at GBs, as shown by arrows in Fig. 2(b), and γ' precipitates. According to previous investigations [16], the γ' precipitates homogeneously dispersed within the γ matrix and had an average size of around 18 ± 3 nm. The volume fraction of γ' after aging treatment was around 17%.

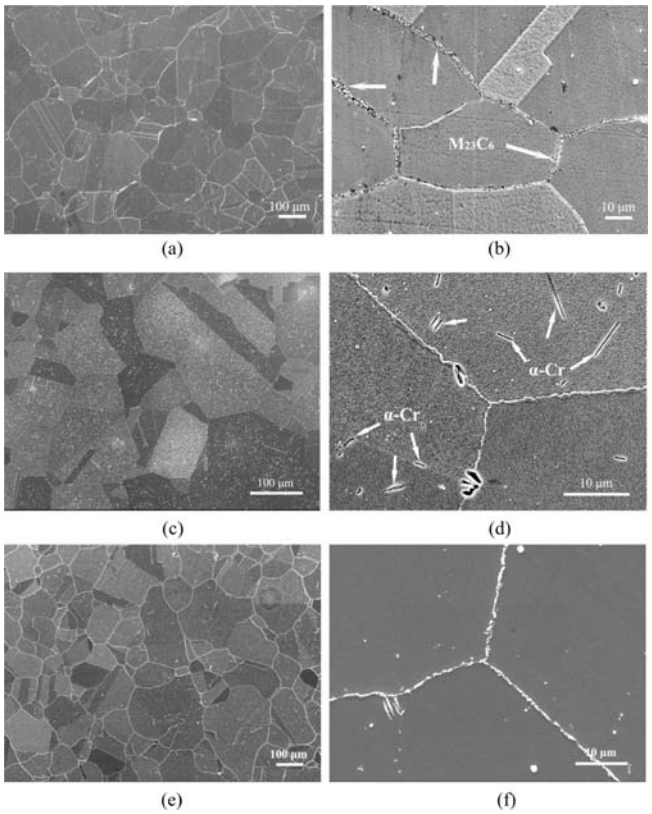

Fig. 2. SEM images showing the microstructures at two length scales after the following heat treatments: (a), (b) H1A1; (c), (d) H1A1+750 °C/5400 h; and (e), (f) H1A1+800 °C/4 h.

Additional thermal exposure at 750 °C for 5400 h results in the formation of α-Cr, as seen in Figs. 2(c) and (d). The area fraction of α-Cr measured using Image-Pro software is approximately 2%, and the average length is 2-5 μm. This phase has been confirmed using selected area electron diffraction and energy dispersive spectrum in the previous observations [16]. In contrast, thermal exposure at 800 °C for 4 h causes no significant change to the microstructure, as shown in Figs. 2(e) and (f). Obviously, the growth and/or coarsening of γ' precipitates occur during thermal exposure, and the size of the γ' precipitates depends on the temperature and time to which they were exposed.

3.3. Deformation microstructures after tensile testing

Figure 3 shows the microstructures of aged specimens after tensile testing at RT. The deformation was heterogeneous, and two main slip systems were activated, as shown in Fig. 3(a). Numerous dislocation slip bands intersected, and each of them consisted of a high density of dislocations. However, the dislocation density in between the slip bands was very low. In Fig. 3(b), many dislocations surrounded the carbides at the grain boundary, indicating that they effectively impede dislocation motion.

After 5400 h of thermal exposure at 750 °C, the tensile deformation microstructures at RT have changed, as shown in Fig. 4. First, the coarsening of the γ' precipitates occurred after long-term thermal exposure. The average size of the γ' precipitates was 122 ± 27 nm, as seen in Fig. 4(a). Second,

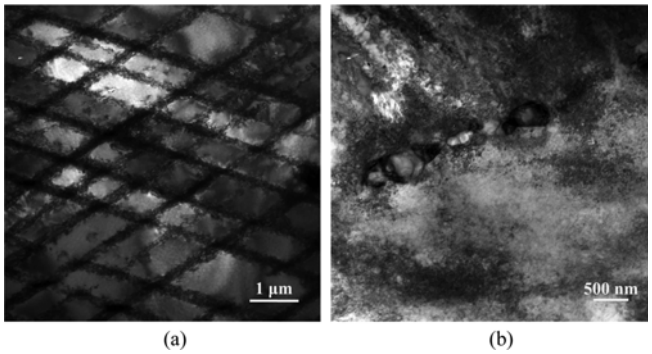

Fig. 3. Microstructures of the aged specimen after tensile deformation at RT at two length scales.

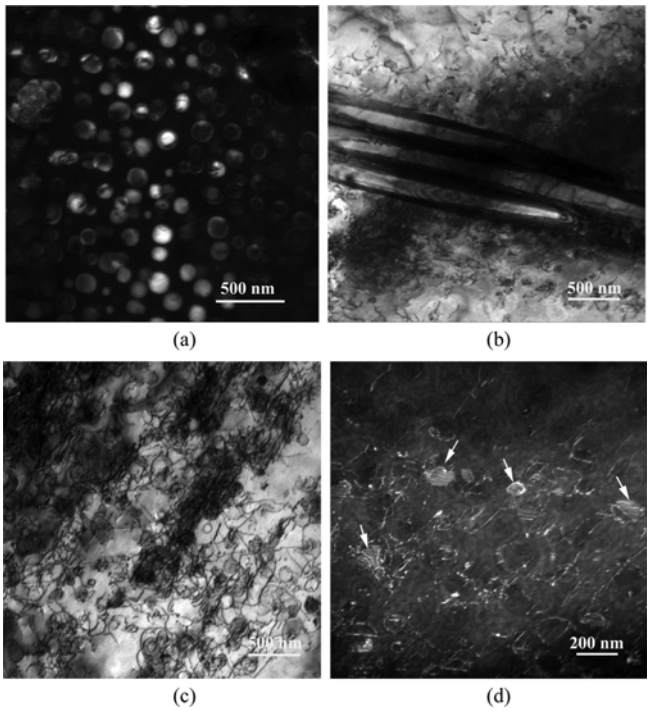

Fig. 4. Tensile deformation microstructures at RT. The specimen was aged and then subjected to long-term thermal exposure at 750 °C for 5400 h. (a) The coarsening of γ' precipitates occurred, and their average size was 122 ± 27 nm. (b) The plate-like α-Cr precipitated in the γ matrix. (c) Dislocations interacted with γ' precipitates via Orowan process. (d) Few stacking faults were observed in the γ' precipitates, as shown by the arrows (note the differing length scale for (d)).

the plate-like α-Cr precipitated in the γ matrix, see Fig. 4(b). Third, the dislocations mainly interacted with the γ' precipitates via the Orowan process. Many dislocation loops around the γ' precipitates can be observed in Fig. 4(c), and only few stacking faults (SFs), see Fig. 4(d), were present in the γ' precipitates.

Figure 5 shows the microstructures of aged specimens after tensile deformation at 750 °C. Compared to the aged specimens deformed at RT, the number of dislocation slip bands was much lower, and they were formed on one slip system.

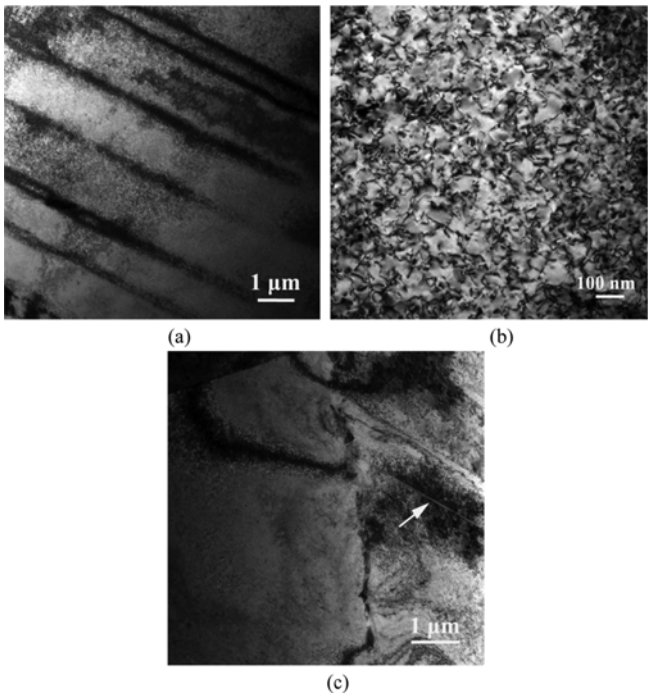

Fig. 5. Microstructures of the aged specimen after tensile deformation at 750 °C. (a) Dislocation slip bands formed on one slip system. (b) Dislocations homogeneously distributed in between slip bands (note the difference in scale for (b)). (c) Few deformation twins were observed; an example of one is indicated by the white arrow.

Dislocations were homogeneously distributed in between slip bands, as seen in Figs. 5(a) and (b). A few deformation twins were observed, as indicated by the arrow in Fig. 5(c).

For the specimens that underwent aging treatment plus 5400 h thermal exposure at 750 °C, their tensile deformation microstructures at 700 °C and at RT are similar. No dislocation slip bands were formed. It seems that the α-Cr phase also served as a dislocation barrier, as seen in Fig. 6(a). Both dislocations looping around the γ' precipitates, and SFs created in the γ' precipitates, can be seen in Figs. 6(b) and (c). The morphology of the γ' precipitates in Fig. 6(d) indicates that no shearing process took place via $a/2<110>$ dislocations.

3.4. Deformation microstructures after creep rupture

The deformation microstructures after creep rupture are illustrated in Figs. 7-9. At 700 °C and 300 MPa, sinuous dislocations were observed in the specimen after aging treatment, see Fig. 7(a), which implies dislocation slip combined with climb. The average size of the γ' precipitates after creep rupture was 33 ± 6 nm. The specimen that was thermally exposed at 800 °C for 4 h after creep rupture at 700 °C and 300 MPa had a similar dislocation structure to the aged specimen. The carbides at the GBs were still isolated. At 750 °C and 150 MPa, the aged specimen after creep rupture showed similar deformation microstructures with those crept at 700 °C and 300 MPa, as

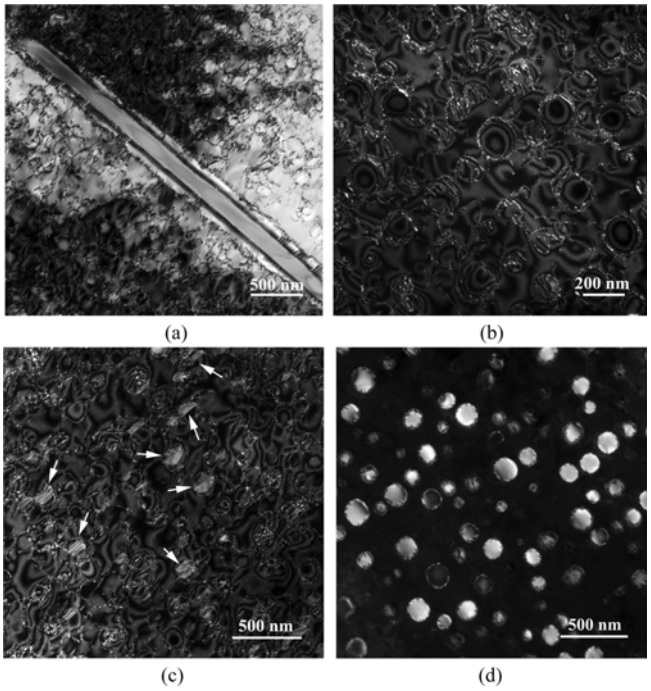

Fig. 6. Microstructures after tensile deformation at 700 °C. The specimen was aged and subjected to long-term thermal exposure at 750 °C for 5400 h. (a) No dislocation slip bands were formed. Many dislocations accumulated at the α-Cr/γ interface. TEM dark filed images showing (b) dislocations looping around the γ' precipitates and (c) SFs created in the γ' precipitates, as indicated by the arrows (note the differing length scale for (b)). (d) The morphology of γ' precipitates indicated no shearing process via *a*/2<110> dislocations.

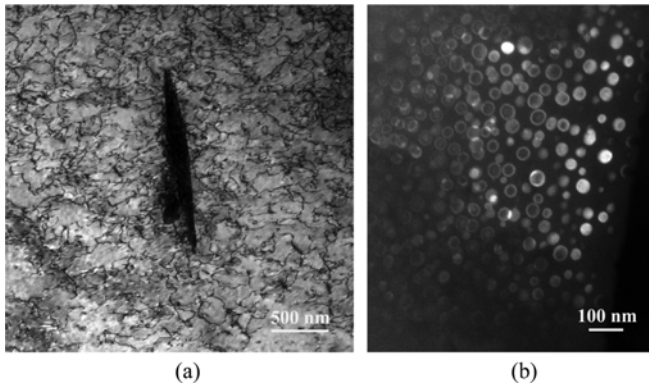

Fig. 7. Deformation microstructures of aged specimens after creep rupture at 700 °C and 300 MPa at different length scales. (a) Sinuous dislocations were present, implying dislocation slip combined with climb. (b) The average size of γ' precipitates after creep rupture was 33 ± 6 nm.

seen in Fig. 9(a). In Fig. 9(b), dislocations interacted with plate-like carbides, and many dislocation loops can be observed.

3.5. Discussion

Compared with previous investigations, the present study showed different characteristics of the deformation processes. For aged specimens tensile tested at RT, thermally

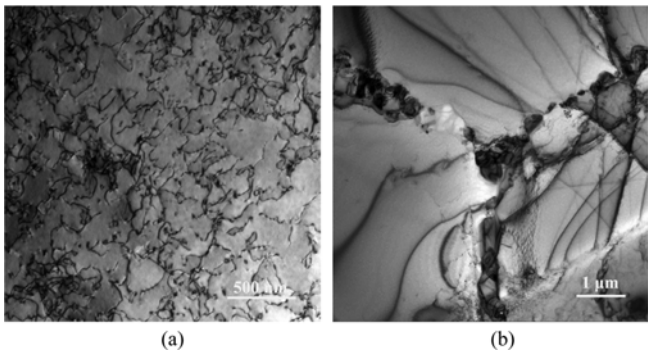

Fig. 8. Deformation microstructures of specimen with aging treatment and subjected to thermal exposure at 800 °C for 4 h after creep rupture at 700 °C and 300 MPa at different length scales. (a) Dislocation slip combined with climb was the dominant mechanism. **(**b) Isolated carbides are visible at grain boundaries.

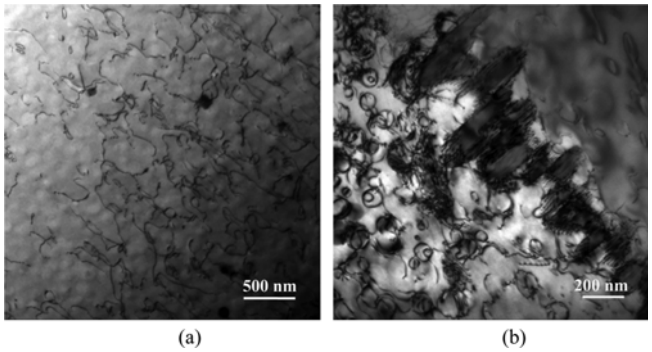

Fig. 9. Microstructures of aged specimens after creep rupture at 750 °C and 150 MPa at different length scales. (a) Sinuous dislocations were observed within the grain. (b) Dislocation interacted with plate-like carbides. Many dislocation loops were present.

assisted dislocation slip is suppressed, and the deformation is more heterogeneous. For the specimen exposed at 750 °C for 5400 h, the average γ' precipitates size was 122 ± 27 nm, almost twice that of the specimen exposed at 700 °C for 7000 h (65 ± 11 nm), which implies a higher coarsening rate of the γ' precipitates. Owing to the larger γ' precipitates, the Orowan process is more prominent, and the extent to which coupled dislocations undergo a shearing process decreases. This difference causes a lower observed yield strength, 656 MPa at RT and 480 MPa at 700 °C, for the specimen exposed at 750 °C for 5400 h compared to the specimen exposed at 700 °C for 7000 h (664 MPa at 700 °C). The related results are discussed below in detail.

The coarsening of the γ' precipitates occurred during thermal exposure. The average γ' size was statistically measured using TEM dark field image. For thermal exposure of 3100 h (TEM results not shown here) and 5400 h at 750 °C, the γ' size was 102 ± 16 nm and 122 ± 27 nm, respectively. The cube of γ' size as a function of exposure time at 750 °C is plotted in Fig. 10, where r and r_0 denote the γ' size after thermal exposure and after aging treatment, respectively. It is seen

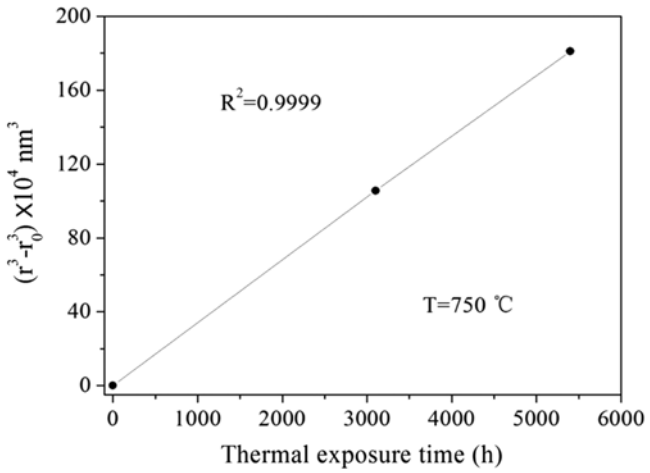

Fig. 10. The cube of γ' size as a function of thermal exposure time at 750 °C; r and r_0 denote the γ' size after thermal exposure and aging treatment, respectively.

that the cube of γ' size is linear with the thermal exposure time. This relationship is in good agreement with the Lifshitz-Slyozov-Wagner theory describing the diffusion-controlled coarsening process in a multi-particle system [19, 20].

For tensile deformation at RT, intersected dislocation slip bands were formed in the aged specimen. Actually, the slip bands consisted of a high density of coupled dislocations that sheared the γ' precipitates. Long-term thermal exposure at 750 °C for 5400 h causes the coarsening of the γ' precipitates. The average size increases from 18 ± 3 nm to 122 ± 27 nm. Thus, the Orowan process is favored due to the increased inter-particle spacing. The critical resolved shear stress required for Orowan bowing is smaller than that required for the shearing process [21,22]. Consequently, the thermally exposed specimen has a lower yield stress (656 MPa) than the aged specimen (787 MPa).

For tensile deformation at elevated temperatures, dislocation climb assists the dislocation slip over the γ' precipitates. The number of dislocation slip bands in the aged specimen tensile tested at 750 °C was much lower than the number in the specimen tested at RT; additionally, the dislocation slip bands were formed on one slip system for the aged specimen tensile tested at 750 °C. Dislocations were homogeneously distributed between slip bands. This could be partly attributed to the increased extent of thermally assisted dislocation climb.

For the specimen thermally exposed at 750 °C for 5400 h, SFs were formed in the γ' precipitates while tensile testing at both RT and 700 °C. Generally, the γ' shearing process is governed by the size, distribution, the anti-phase boundary energy and stacking fault energy of γ' precipitates. The present investigation used the same alloy and thermal exposure caused size variation in the γ' precipitates. Thus, precipitate size is thought to play an important role in the γ' shearing process. Because of large precipitate size, dislocations may not have enough time to climb over the precipitates due to rapid deformation. Consequently, stress concentration occurs at the γ/γ' interface as deformation strain increases. It is believed that the stress accumulation due to large precipitate size and increased strain facilitates the dislocation dissociation. This phenomenon was also observed in the previous investigations [16]. In those studies, the specimen was aged and subjected to thermal exposure at 700 °C for 7000 h, and the γ' precipitates had a size of 65 ± 11 nm. For the Ni-based superalloys, partial dislocations shearing the γ' precipitates and creating SFs in the γ' precipitates are important mechanisms [23-27], which depends on not only the materials characteristics but also on the deformation conditions.

The creep mechanisms under conditions of 700 °C/300 MPa and 750 °C/150 MPa are similar. There is no shearing process (dislocations cutting through the γ' precipitates) observed because of the low critical resolved shear stress. Dislocation slip combined with climb is the dominant mechanism. For the present case, critical resolved shear stress might not be large enough to solely activate the Orowan process. There are two factors that facilitate the Orowan process. First, the force of the dislocation interaction is what pushes the dislocation to move forward. The value of the interaction force depends on the dislocation density. Second, dislocation climb also assists the Orowan process. For the specimen exposed at 800 °C for 4 h, note that though it has shorter creep rupture life than the aged specimen at 700 °C and 300 MPa, the creep strain up to approximately 220 h is relatively lower. This phenomenon could be explained as follows: the thermally exposed specimen has larger γ' precipitates than the aged one. Initially, the creep strain is small, and the dislocation density is low. Therefore, the dislocation interaction is not strong. At this stage, the second factor, dislocation climb, may dominate the creep. Thus, larger γ' precipitate size (longer climb time) causes lower creep stain. As the creep deformation proceeds, the dislocation interaction becomes stronger, and the first factor may make more contributions to an Orowan process. In this case, the bigger γ' precipitate size, the larger inter-precipitate spacings become. Thus, for the thermally exposed specimen with bigger γ' precipitate size, an Orowan looping process assisted by dislocation interaction is relatively easier, which results in a large creep strain in the later creep stage.

4. CONCLUSIONS

A newly developed Ni-Fe-based superalloy, HT-X, was subjected to various heat treatments. Tensile tests were conducted at RT and elevated temperatures. Creep tests were carried out under conditions of 700 °C/300 MPa and 750 °C/150 MPa. After mechanical testing, the deformation microstructures were investigated using TEM. The following conclusion can be drawn.

(1) After aging treatment, the yield strength of the HT-X alloy at RT and 750 ℃ was 787 MPa and 624 MPa, respectively. When the alloy was exposed at 750 °C for 5400 h, its yield strength was decreased to 656 MPa at RT and 480 MPa at 700 °C.

(2) The size of the γ' precipitates plays an important role in tensile deformation. For the aged specimen with a γ' precipitate size of 18 ± 3 nm, the $a/2<110>$ dislocation shearing process occurred when tensile tested at RT and 750 °C. When the γ' precipitate size was increased to 122 ± 27 nm (exposed at 750 °C for 5400 h), the Orowan process became dominant, and SFs were created in the γ' precipitates at both RT and 700 °C.

(3) At 700 °C and 300 MPa, additional thermal exposure at 800 °C for 4 h after aging treatment reduced the creep rupture life. At 750 °C and 150 MPa, the aged specimen had a creep rupture life of 2768 h. For all three specimens, the total creep strain was less than 3.0%.

(4) The creep mechanisms did not vary significantly under the tested conditions. Generally, dislocation slip combined with climb is the dominant mechanism for the tested conditions.

ACKNOWLEDGMENTS

This work has been financially supported by the China Huaneng group, Huaneng Power International, Inc., and the Natural National Science Foundation of China under Grant no. 51301130, 51301131 and 51401071.

REFERENCES

1. C. G. Stolzenberger, *Energy Mater.* **2**, 141 (2007).
2. S. Z. Li, Z. Eliniyaz, L. T. Zhang, F. Sun, Y. Z. Shen, and A. D. Shan, *Mater. Charact.* **73**, 144 (2012).
3. D. B. Park, S. M. Hong, K. H. Lee, M. Y. Huh, J. Y. Suh, S. C. Lee, and W. S. Jung, *Mater. Charact.* **93**, 52 (2014).
4. G. S. Shin, J. Y. Yun, M. C. Park, and S. J. Kim, *Mater. Charact.* **95**, 180 (2014).
5. R. Viswanathan, K. Coleman, and U. Rao, *Int. J. Press. Vessel. Pip.* **83**, 778 (2006).
6. N. D. Evans, P. J. Maziasz, R. W. Swindeman, and G. D. Smith, *Scr. Mater.* **51**, 503 (2004).
7. Y. Chong, Z. D. Liu, G. Andy, W. Liu, and Y. Q. Weng, *Mater. Sci. Eng. A* **589**, 153 (2014).
8. Q. Y. Wu, H. J. Song, R. W. Swindeman, J. P. Shingledecker, and V. K. Vasudevan, *Metall. Mater. Trans. A* **39**, 2569 (2008).
9. R. Krishna, S. V. Hainsworth, H. V. Atkinson, and A. Strang, *Mater. Sci. Technol.* **26**, 797 (2010).
10. M. Akbari-Garakani and M. Mehdizadeh, *Mater. Des.* **32**, 2695 (2011).
11. P. S. Weitzel, J. M. Tanzosh, B. Boring, N. Okita, T. Takahashi, and N. Ishikawa, *Advanced Ultra-supercritical Power Plant (700 to 760C) Design for Indian Coal*, http://www.babcock.com/library/documents/br-1884.pdf (accessed December 5, 2014).
12. L. G. Klingensmith, *Proceedings of the 4th Symposium on Heat Resistant Steels and Alloys for High Efficiency USC Power Plants*, pp.307-321, China (2011).
13. J. P. Shingledecker and N. D. Evans, *Intl. J. Press. Vessel Pip.* **87**, 345 (2010).
14. H. Semba, H. Okada, T. Hamagushi, S. Ishikawa, and M. Yoshizawa, *Technical Report of Nippon Steel & Sumitomo Metal* **397**, 71 (2013).
15. T. T. Wang, C. S. Wang, J. T. Guo, and L. Z. Zhou, *Mater. Sci. Forum* **747-748**, 647 (2013).
16. Y. Yuan, Z. H. Zhong, Z. S. Yu, H. F. Yin, Y. Y. Dang, X. B. Zhao, Z. Yang, J. T. Lu, J. B. Yan, and Y. Gu, *Mater. Sci. Eng. A* **619**, 364 (2014).
17. Y. F. Gu, Y. Yuan, X. B. Zhao, J. T. Lu, J. B. Yan, Y. Y. Dang, Z. Yang, H. Y. Yin, and C. X. Fan, *Proc. of APEC Expert Workshop on Innovative Systemic Approaches to Enhancing Coal-Fired Power Generation Efficiency* (eds. Z. X. Wang, F. Wang), p.175, China Energy Research Society, China (2015).
18. J. T. Guo and X. K. Du, *Acta Metall. Sinica* **41**, 1221 (2005).
19. M. Lifshitz and V. V. Slyozov, *J. Phys. Chem. Solids* **19**, 35 (1961).
20. C. Wagner, *Z. Elektrochem.* **65**, 581 (1961).
21. B. Reppich, *Acta Metall.* **30**, 87 (1982).
22. B. Reppich, P. Schepp, and G. Wehner, *Acta Metall.* **30**, 95 (1982).
23. K. Gopinath, A. K. Gogia, S. V. Kamat, R. Balamuralikrishnan, and U. Ramamurty, *Metall. Mater. Trans. A* **39**, 2340 (2008).
24. Y. Yuan, Y. F. Gu, T. Osada, Z. H. Zhong, T. Yokokawa, and H. Harada, *Scr. Mater.* **67**, 137 (2012).
25. R. R. Unocic, G. B. Viswanathan, P. M. Sarosi, S. Karthikeyan, J. Li, and M. J. Mills, *Mater. Sci. Eng. A* **483-484**, 25 (2008).
26. G. B. Viswanathan, P. M. Sarosi, M. F. Henry, D. D. Whitis, W. W. Milligan, and M. J. Mills, *Acta Mater.* **53**, 3041 (2005).
27. S. Raujol, M. Benyoucef, D. Locq, P. Caron, F. Pettinari, N. Clement, and A. Coujou, *Philos. Mag.* **86**, 1189 (2006).